DOA and Gain-Phase Errors Estimation for Noncircular Sources With Central Symmetric Array

Wei Xie, *Student Member, IEEE*, Changsheng Wang, *Student Member, IEEE*, Fei Wen, *Member, IEEE*, Jiangbo Liu, *Student Member, IEEE*, and Qun Wan, *Member, IEEE*

Abstract—The problem of direction-of-arrival (DOA) estimation for noncircular sources impinging on a central symmetric array (CSA) in the presence of sensor gain-phase uncertainties is addressed in this paper. A noniterative method is proposed and the corresponding stochastic Cramér–Rao bound is derived. The proposed method is realized through two steps. First, an eigenstructure-based technique is presented to estimate the spatial signatures. Second, the DOAs are obtained by adopting an element-wise division approach to the estimated spatial signatures, based on which, the sensor gain-phase errors are given in closed-form. The ambiguity of DOA estimation is analyzed as well. The proposed method offers a number of advantages in comparison with the existing methods that apply to CSA. First, the DOA estimator is independent of the sensor phases. Second, the proposed method applies to incoherent sources. Third, the proposed method is capable of providing 360° azimuthal coverage under certain conditions. Fourth, an additional performance gain is achieved by taking the property of noncircular sources into consideration. Numerical simulations are provided to verify the effectiveness of the proposed method.

Index Terms—Direction-of-arrival (DOA), central symmetric array (CSA), gain-phase errors, noncircular signal, spatial signature.

I. INTRODUCTION

THE problem of direction-of-arrival (DOA) estimation by combining the received data from an array of sensors has been an important topic in many applications, such as radar, sonar and mobile communication. Many advanced DOA estimation techniques, such as subspace-based methods like MUSIC [1], ESPRIT [2] and their derivatives [3]–[5], could achieve super-resolution. But, an inherent assumption of these methods is that the sensor gains and phases are perfectly known. Otherwise, the estimator'¡¯s performance could degrade substantially [6]. Nevertheless, in practical

application, the gain-phase errors always exist since the sensor characteristics may shift with the time and the environment.

To deal with the uncertainties of sensor gains and phases, a number of algorithms have been proposed. For example, a kind of pre-calibration techniques have been presented in [7]–[10]. These methods require that all the DOAs are precisely known. When this condition is satisfied, the array can be calibrated well. However, considering the difficulties to obtain an accurate DOA [11] and the time-variation characteristic of sensor gains and phases, an auto-calibration method is more preferred in practice.

The auto-calibration methods jointly estimate the parameters of DOA and gain-phase errors. In [12], an simple but effective iterative method is proposed. But it requires that the array perturbations are small. Based on the assumption that the array perturbations are drawn from a Gaussian distribution, [13], [14] present a maximum-a-posteriori (MAP) method and a weighted noise subspace fitting (WNSF) method, respectively. These two methods have an excellent performance. However, they require multidimensional search and suffer from suboptimal convergence. Based on the amplitude-only measurements, [15], [16] present two noniterative algorithms. However, these two methods require that the source signals are uncorrelated with each other and the DOAs are confined in [−90°, 90°]. The aforementioned methods [12]–[16] are not designed for any specific array configuration, and then apply to arbitrary array geometries. To overcome the above listed limitations, one may make use of the properties of the array geometries to derive more suitable algorithms. For example, uniformly linear array (ULA), partly calibrated ULA and uniform rectangular array (URA) are studied in [17]–[23]. Meanwhile, some efficient auto-calibration algorithms are proposed in these works.

In practical applications, various array geometries belonging to central symmetric array (CSA), such as ULA, uniformly circular array (UCA) with even antennas number, cross shaped array and URA, are widely used. Algorithms like the methods in [24]–[26] are specially designed for CSA to improve the DOA estimation performance. On the other hand, noncircular signals, including amplitude modulated (AM), M-ary amplitude shift keying (MASK) and binary phase shift keying (BPSK) signals [27], are usually encountered in the context of radio communications. Compared to the circular signals, the second-order statistics (SOS) of

which are uniquely determined by its covariance matrix, the SOS of the noncircular signals are additionally determined by its conjugate covariance matrix. It has been shown in [26] and [28]–[30] that a significant gain in terms of DOA estimation performance can be achieved by making full use of the SOS of noncircular signals. Thus, it naturally makes sense to take the second-order noncircularity and the structure of array geometry into account to design more suitable auto-calibration algorithm.

In this paper, we consider the problem of jointly estimating the DOAs and gain-phase errors for noncircular sources with CSA. A two steps method is proposed. First, the spatial signatures are estimated by extending the technique in [31], which is specially designed for ULA. Second, the DOAs are obtained by finding the peak(s) of the two-dimensional spectrum that constructed by element-wise division of the spatial signatures. The sensor gain-phase errors are straightforwardly obtained by using the estimated DOAs and spatial signatures. The step of DOA estimation is independent of the sensor phase errors, which is similar to the amplitude-only measurements based techniques [15], [16]. However, there are much more ambiguous points in the two-dimensional spectra of these two methods, which brings additional difficulties to identify the DOAs, and then, less sources can be handled. In this paper, we also provide an analysis on the relationship between the true DOAs and the ambiguous points. Meanwhile, a simple method is provided to solve the problem of ambiguity. Thus, the proposed method is capable of providing 360° azimuthal coverage under certain conditions. We also derive the corresponding stochastic Cramér-Rao bound (CRB) to which we compare the performance of the proposed method. Simulation results demonstrate a substantially improved estimation performance of the proposed method as compared to the traditional techniques in [12] and [16].

The rest of this paper is organized as follows. In Section II, the problem is formulated. The proposed method is given, and the ambiguity is analyzed in Section III. In Section IV, a relevant stochastic CRB is derived. Section V contains simulation results. Conclusions are given in Section VI.

Throughout this paper, the following notations are used. The superscriptions $*$, T, H and $\dagger$ denote the conjugate, transpose, Hermitian transpose and pseudo-inverse, respectively. The notations $E\{\cdot\}$, $\|\cdot\|$, $\Re(\cdot)$, $\mathrm{Tr}(\cdot)$, $\det(\cdot)$, $\odot$, $\oslash$ and $\otimes$ stand for the expectation, Frobenius norm, real part, trace, determinant, Hadamard product, Hadamard division and Kronecker product, respectively. $\mathbf{D}(\mathbf{x})$ represents the diagonal matrix with $\mathbf{x}$ in its main diagonal. $\mathbf{I}_M$, $\boldsymbol{\Gamma}$, $\mathbf{1}_{m,n}$ and $\mathbf{0}$ denote the $M \times M$ identify matrix, the $M \times M$ exchange matrix, the $m \times n$ matrix of 1s and the matrix of 0s with a appropriate dimension unless otherwise specified, respectively. Finally, $\hat{\cdot}$ stands for the estimated term.

II. PROBLEM FORMULATION

Consider K far-field narrow-band signals $s_1(t)$, $s_2(t)$, ..., $s_K(t)$ impinging on a planar array of M omnidirectional sensors from directions θ_1, θ_2, ..., θ_K. Suppose that the array is uncalibrated with sensor gains ρ_1, $\rho_2, \ldots, \rho_M$ and phases ϕ_1, ϕ_2, ..., ϕ_M. Without loss of generality, let the

sensor 1 be taken as the reference, then we have $\rho_1 = 1$ and $\phi_1 = 0$. Arranging these parameters in vector form as $\mathbf{s}(t) = [s_1(t), s_2(t), \ldots, s_K(t)]^T$, $\boldsymbol{\theta} = [\theta_1, \theta_2, \ldots, \theta_K]^T$, $\boldsymbol{\rho} = [\rho_1, \rho_2, \ldots, \rho_M]^T$ and $\boldsymbol{\phi} = [\phi_1, \phi_2, \ldots, \phi_M]^T$, the array output at time t can be modeled as

$$\mathbf{y}(t) = \mathbf{D}(\mathbf{g})\mathbf{A}\mathbf{s}(t) + \mathbf{n}(t) = \mathbf{B}\mathbf{s}(t) + \mathbf{n}(t), \qquad (1)$$

where $\mathbf{A} = [\mathbf{a}(\theta_1), \mathbf{a}(\theta_2), \ldots, \mathbf{a}(\theta_K)]$ is the array manifold with $\mathbf{a}(\theta)$ denoting the steering vector towards direction θ, $\mathbf{n}(t) \in \mathbb{C}^{M \times 1}$ is additive noise, $\mathbf{g} = \boldsymbol{\rho} \odot \exp(j\boldsymbol{\phi}) = [g_1, g_2, \ldots, g_M]^T$ and $\mathbf{B} = \mathbf{D}(\mathbf{g})\mathbf{A} = [\mathbf{b}_1, \mathbf{b}_2, \ldots, \mathbf{b}_K]$ is the spatial signature matrix with $\mathbf{b}_k = \mathbf{D}(\mathbf{g})\mathbf{a}(\theta_k)$ denoting the spatial signature of the kth source. It is assumed that the noise vector $\mathbf{n}(t)$ is a circular Gaussian process with mean zero and covariance $\sigma_n^2 \mathbf{I}_M$ with σ_n^2 denoting the noise power, and uncorrelated with $\mathbf{s}(t)$, i.e., $E\{\mathbf{n}(t)\mathbf{s}^T(t)\} = E\{\mathbf{n}(t)\mathbf{s}^H(t)\} = \mathbf{0}$. The steering vector towards the direction θ_k is given (element-wise) by

$$[\mathbf{a}(\theta_k)]_m = \exp\left(-j\omega(x_m \sin\theta_k + y_m \cos\theta_k)\right), \qquad (2)$$

where (x_m, y_m) denotes the coordinate of the kth antenna and $\omega = 2\pi/\lambda$ with λ denoting the wavelength. Suppose that the array has a central-symmetric structure and let the array centroid be the coordinate origin. It is easy to verify that the array manifold satisfies

$$\mathbf{A} = \boldsymbol{\Gamma}\mathbf{A}^*. \qquad (3)$$

The incident signals are assumed to be strict sense noncircular (SSNC). Thus, $s_k(t)$ ($k \in \{1, 2, \ldots, K\}$) can be expressed by the product of a complex scalar $\exp(j\alpha_k/2)$ and a real-valued signal $\bar{s}_k(t)$, where α_k is the noncircular phase of $s_k(t)$. Then, we can write

$$\mathbf{s}(t) = \mathbf{D}(\boldsymbol{\beta})\bar{\mathbf{s}}(t), \qquad (4)$$

where $\bar{\mathbf{s}}(t) = [\bar{s}_1(t), \bar{s}_2(t), \ldots, \bar{s}_K(t)]^T$ and $\boldsymbol{\beta} = \exp(j\boldsymbol{\alpha}/2)$ with $\boldsymbol{\alpha} = [\alpha_1, \alpha_2, \ldots, \alpha_K]^T$.

To take advantage of the properties carried by the incident signals and the array, we augment the array output as

$$\bar{\mathbf{y}}(t) = [\mathbf{y}^T(t), (\boldsymbol{\Gamma}\mathbf{y}(t))^H]^T = \bar{\mathbf{B}}\bar{\mathbf{s}}(t) + \bar{\mathbf{n}}(t), \qquad (5)$$

where $\bar{\mathbf{n}}(t) = [\mathbf{n}^T(t), (\boldsymbol{\Gamma}\mathbf{n}(t))^H]^T$ and

$$\bar{\mathbf{B}} = \begin{bmatrix} \mathbf{B}\mathbf{D}(\boldsymbol{\beta}) \\ \boldsymbol{\Gamma}\mathbf{B}^*\mathbf{D}(\boldsymbol{\beta}^*) \end{bmatrix} = \begin{bmatrix} \mathbf{B}\mathbf{D}(\boldsymbol{\beta}) \\ g_0 \mathbf{D}(\bar{\mathbf{g}})\mathbf{B}\mathbf{D}(\boldsymbol{\beta}^*) \end{bmatrix} = \begin{bmatrix} \mathbf{B}_1 \\ \mathbf{B}_2 \end{bmatrix} \qquad (6)$$

with $\bar{\mathbf{g}} = g_0^{-1}\boldsymbol{\Gamma}\mathbf{g}^* \oslash \mathbf{g} = [\bar{g}_1, \bar{g}_2, \ldots, \bar{g}_M]^T$ and $g_0 = g_M^*$. Clearly, we have $\bar{g}_1 = 1$.

The augmented array covariance matrix is given by

$$\mathbf{R}_{\bar{y}} = E\{\bar{\mathbf{y}}(t)\bar{\mathbf{y}}^H(t)\} = \bar{\mathbf{B}}\mathbf{R}_s\bar{\mathbf{B}}^H + \sigma_n^2\mathbf{I}_{2M}, \qquad (7)$$

with $\mathbf{R}_s = E\{\bar{\mathbf{s}}(t)\bar{\mathbf{s}}^T(t)\} \in \mathbb{R}^{K \times K}$. The eigenvalue decomposition (EVD) of $\mathbf{R}_{\bar{y}}$ is given by

$$\mathbf{R}_{\bar{y}} = \mathbf{U}_s\boldsymbol{\Sigma}_s\mathbf{U}_s^H + \mathbf{U}_n\boldsymbol{\Sigma}_n\mathbf{U}_n^H, \qquad (8)$$

where the diagonal matrices $\boldsymbol{\Sigma}_s$ and $\boldsymbol{\Sigma}_n$ consist of the K largest and the $2M - K$ smallest eigenvalues of $\mathbf{R}_{\bar{y}}$, respectively, $\mathbf{U}_s \in \mathbb{C}^{2M \times K}$ spans the signal subspace whose columns are the eigenvectors corresponding to the K largest eigenvalues, and

$\mathbf{U}_n \in \mathbb{C}^{2M \times (2M-K)}$ spans the noise subspace whose columns are the eigenvectors corresponding to the $2M - K$ smallest eigenvalues.

Assume that the source covariance matrix $\mathbf{R}_s$ is nonsingular, and the sources number K is known or has been estimated by the existing method [3]. Based on the known sources number K and the array received data $\{\mathbf{y}(t)\}_{t=1}^T$ with T denoting the number of snapshots, the goal of this paper is to determine the DOAs, the sensor gains and phases, as well as the noncircular phases.

III. PROPOSED METHOD

A. Spatial Signatures Estimation

Based on K and $\{\mathbf{y}(t)\}_{t=1}^T$, only the signal subspace and the noise subspace can be estimated in (8) using the estimated array covariance matrix $\hat{\mathbf{R}}_{\bar{y}} = \sum_{t=1}^T \bar{\mathbf{y}}(t)\bar{\mathbf{y}}^H(t)$. In this subsection, the connection between the spatial signatures and the signal subspace is studied, based on which, a simple method for estimating the spatial signatures is established.

Since $\mathbf{U}_s$ and $\bar{\mathbf{B}}$ span the same space for inherent sources with unambiguous array, there must exist a unique and nonsingular matrix $\mathbf{T} = [\mathbf{t}_1, \mathbf{t}_2, \ldots, \mathbf{t}_K] \in \mathbb{C}^{K \times K}$ such that

$$\mathbf{U}_{s1}\mathbf{T} = \mathbf{BD}(\boldsymbol{\beta}), \tag{9a}$$

$$\mathbf{U}_{s2}\mathbf{T} = g_0\mathbf{D}(\bar{\mathbf{g}})\mathbf{BD}(\boldsymbol{\beta}^*). \tag{9b}$$

where $\mathbf{U}_{s1}, \mathbf{U}_{s2} \in \mathbb{C}^{M \times K}$ satisfy $\mathbf{U}_s = [\mathbf{U}_{s1}^T, \mathbf{U}_{s2}^T]^T$. Clearly, to express the spatial signatures (with possible scaling factors) by $\mathbf{U}_s$, we only need the expression of $\{\mathbf{t}_k\}$.

From (9a), we have $\mathbf{B} = \mathbf{U}_{s1}\mathbf{TD}^{-1}(\boldsymbol{\beta})$. Substituting this back to (9b), we get

$$\mathbf{U}_{s2} = \mathbf{D}(\bar{\mathbf{g}})\mathbf{U}_{s1}\boldsymbol{\Psi}, \quad \boldsymbol{\Psi} = g_0\mathbf{TD}^{-2}(\boldsymbol{\beta})\mathbf{T}^{-1}. \tag{10}$$

In (10), it can be seen that $\boldsymbol{\Psi}$ has the eigenvalues $\{v_k \doteq g_0\beta_k^{-2}\}$ and the eigenvectors $\{\mathbf{t}_k\}$. Moreover, from (10), $\boldsymbol{\Psi}$ can also be expressed as

$$\boldsymbol{\Psi} = \mathbf{U}_{s1}^\dagger \mathbf{D}^{-1}(\bar{\mathbf{g}})\mathbf{U}_{s2}. \tag{11}$$

Substituting (11) back to (10) gives

$$\mathbf{D}^{-1}(\bar{\mathbf{g}})\mathbf{U}_{s2} - \mathbf{P}_{\mathbf{U}_{s1}}\mathbf{D}^{-1}(\bar{\mathbf{g}})\mathbf{U}_{s2}$$
$$= \mathbf{P}_{\mathbf{U}_{s1}}^\perp \mathbf{D}^{-1}(\bar{\mathbf{g}})\mathbf{U}_{s2} = \mathbf{0}, \tag{12}$$

where $\mathbf{P}_{\mathbf{U}_{s1}}^\perp = \mathbf{I}_M - \mathbf{P}_{\mathbf{U}_{s1}}$ and $\mathbf{P}_{\mathbf{U}_{s1}} = \mathbf{U}_{s1}\mathbf{U}_{s1}^\dagger$. It follows that

$$\|\mathbf{P}_{\mathbf{U}_{s1}}^\perp \mathbf{D}^{-1}(\bar{\mathbf{g}})\mathbf{U}_{s2}\|^2$$
$$= \mathrm{Tr}\left(\mathbf{P}_{\mathbf{U}_{s1}}^\perp \mathbf{D}^{-1}(\bar{\mathbf{g}})\mathbf{U}_{s2}\mathbf{U}_{s2}^H\mathbf{D}^{-H}(\bar{\mathbf{g}})\mathbf{P}_{\mathbf{U}_{s1}}^\perp\right)$$
$$= (\mathbf{1}_{M,1} \oslash \bar{\mathbf{g}})^H\mathbf{G}(\mathbf{1}_{M,1} \oslash \bar{\mathbf{g}}) = 0, \tag{13}$$

where $\mathbf{G} = \mathbf{P}_{\mathbf{U}_{s1}}^\perp \odot (\mathbf{U}_{s2}\mathbf{U}_{s2}^H)^T$. (13) implies that $\mathbf{G}$ is rank deficiency, and $\mathbf{1}_{M,1} \oslash \bar{\mathbf{g}} \in \mathrm{null}(\mathbf{G})$. Moreover, we have the following result.

Theorem 1: Under the assumption that the given array is ambiguous, we have that

$$\mathrm{rank}(\mathbf{G}) = M - 1 \tag{14}$$

when $0 < K < M$.

Proof: See Appendix A.   ∎

Partition $\mathbf{G}$ as $\mathbf{G} = [\mathbf{g}_L, \mathbf{G}_R]$ with $\mathbf{g}_L \in \mathbb{C}^{M \times 1}$. We have that $\mathbf{G}_R$ is of full column rank, otherwise, there must exist a nonzero vector $\mathbf{x} \in \mathbb{C}^{(M-1) \times 1}$ such that $[0, \mathbf{x}^T]^T \in \mathrm{null}(\mathbf{G})$. However, the vectors $[0, \mathbf{x}^T]^T$ and $\mathbf{1}_{M,1} \oslash \bar{\mathbf{g}}$ cannot span the same space, since $\bar{g}_1 \neq 0$. Based on this observation, (13) and (14), it is easy to establish that

$$\bar{\mathbf{g}} = \mathbf{1}_{M,1} \oslash [1, -(\mathbf{G}_R^\dagger \mathbf{g}_L)^T]^T. \tag{15}$$

With $\bar{\mathbf{g}}$ and the facts (9)-(11), one can easily establish the algorithm for estimating the spatial signatures by using the estimated signal subspace $\hat{\mathbf{U}}_s = [\hat{\mathbf{U}}_{s1}^T, \hat{\mathbf{U}}_{s2}^T]^T$. The algorithm is outlined as follows.

1) Construct $\mathbf{G}$ by using the estimated signal space $\hat{\mathbf{U}}_{s1}$ and $\hat{\mathbf{U}}_{s2}$ according to (13).
2) Obtain $\hat{\bar{\mathbf{g}}}$ and $\hat{\boldsymbol{\Psi}}$ according to (15) and (11), respectively.
3) Obtain $\{\hat{\mathbf{t}}_k\}$ and $\{\hat{v}_k\}$ by performing the EVD of $\hat{\boldsymbol{\Psi}}$.
4) Estimate the spatial signatures according to (9). Specifically, let $\hat{\mathbf{b}}_k$ be the left singular vector corresponding to the largest singular value of $[\hat{\mathbf{b}}_k^1, \hat{\mathbf{b}}_k^2]$, where

$$\hat{\mathbf{b}}_k^1 = \hat{\mathbf{U}}_{s1}\hat{\mathbf{t}}_k \quad \text{and} \quad \hat{\mathbf{b}}_k^2 = \mathbf{D}^{-1}(\hat{\bar{\mathbf{g}}})\hat{\mathbf{U}}_{s2}\hat{\mathbf{t}}_k. \tag{16}$$

Note that, since the eigenvectors of a matrix are not unique, only scaled spatial signatures can be obtained using the above method even if the noncircular phases are known.

Remark 1: Since the elements of steering vectors all have unit modulus, the sensor gains can be directly obtained by calculating the moduli of the elements of the estimated spatial signatures. Nevertheless, the sensor phases are still intractable. Although $\bar{\mathbf{g}}$ has been estimated, there are only $\lceil M/2 \rceil - 1$ independent equations can be constructed by using the phases of $\{\bar{g}_k\}$, where $\lceil m \rceil$ denotes the minimum integer that is no less than m.

In the above derivation, an implicit assumption is that the noncircular phases of sources are distinct to make sure the eigenvalues of $\boldsymbol{\Psi}$, i.e., $\{v_k\}$, are distinct. Nevertheless, even when some sources have a same noncircular phase, the spatial signatures of the sources with unique noncircular phases can also be determined. It should be noted that, the noncircular phase of a SSNC signal depends on multiple factors, such as transmit delay and carrier phase, which results in a strong randomness of the noncircular phase. Moreover, when all the noncircular phases are the same, if possible, a small shift of the source(s) or the array would result in a relative variation of the noncircular phases (caused by the relative variations of the transmit delays among incident signals).

Let α_k^D be the minimum absolute difference of noncirluar phases among the kth source to the others, i.e.,

$$\alpha_k^D = 2 \min_{q, q \neq k}\{|\angle(\beta_k\beta_q^*)|\} = \min_{q, q \neq k}\{|\angle(v_k^*v_q)|\}, \tag{17}$$

where $\angle(\cdot)$ and $|\cdot|$ denote the complex angle and the absolute value, respectively. Without loss of generality, we assume that

$$\alpha_1^D \geq \alpha_2^D \geq, \ldots, \geq \alpha_K^D. \tag{18}$$

Obviously, the estimated spatial signature of the first source must be most reliable compared to the other sources, and it can be identified by (17) using the estimated values $\{\hat{v}_k\}$.

B. DOA and Gain-Phase Errors Estimation

To estimate the DOAs, based on $\hat{\mathbf{B}} = [\hat{\mathbf{b}}_1, \hat{\mathbf{b}}_2, \ldots, \hat{\mathbf{b}}_K]$, the methods in [15] and [16] are applicable when $K(K-1) < M$ and the DOAs are confined in the range of $[-90°, 90°]$. To cope with the limitations of these methods, an element-wise division approach is proposed in this subsection for estimating the DOAs, with which the sensor gain-phase errors and noncircular phases are obtained in closed-form.

Assume that the signal subspace is perfectly estimated, and $\alpha_1^D > 0$. Then, $\hat{\mathbf{b}}_1$ can be expressed as

$$\hat{\mathbf{b}}_1 = \varepsilon_1 \mathbf{D}(\mathbf{g})\mathbf{a}(\theta_1), \qquad (19)$$

where ε_1 is the unknown scaling factor of the first source. Construct

$$\mathbf{E} = \mathbf{D}^{-1}(\hat{\mathbf{b}}_1)[\hat{\mathbf{b}}_2, \hat{\mathbf{b}}_3, \ldots, \hat{\mathbf{b}}_K] \in \mathbb{C}^{M \times (K-1)}, \qquad (20)$$

and let $\mathbf{E}_n \in \mathbb{C}^{M \times (M-K+1)}$ consist of the left singular vectors corresponding to the $M - K + 1$ smallest singular values of $\mathbf{E}$. Clearly, regardless of the values of $\{\alpha_k^D\}_{k>1}$, we have

$$\begin{aligned} \mathrm{span}(\mathbf{E}_n) &= \mathrm{null}(\mathbf{E}^H) \\ &= \mathrm{null}\left(\left[\mathbf{a}(\theta_2) \oslash \mathbf{a}(\theta_1), \ldots, \mathbf{a}(\theta_K) \oslash \mathbf{a}(\theta_1)\right]^H\right). \end{aligned} \qquad (21)$$

It follows that the vectors $\mathbf{a}(\theta_k) \oslash \mathbf{a}(\theta_1)$, $k = 1, 2, \ldots, K-1$, are orthogonal to $\mathbf{E}_n$. Consequently, we could construct the following function for DOA estimation:

$$f(\theta, \varphi) = \frac{1}{\left\| \mathbf{E}_n^H \left(\mathbf{a}(\theta) \oslash \mathbf{a}(\varphi)\right) \right\|^2}. \qquad (22)$$

If there is no ambiguity, then all the K DOAs can be identified via finding the $K - 1$ largest peaks of $f(\theta, \varphi)$.

Unfortunately, even if the given array is unambiguous, the function $f(\theta, \varphi)$ also exists DOA ambiguity in the searching range from $-180°$ to $180°$ for both the variables θ and φ. Similar to the ambiguity analysis of the array manifold, the DOA ambiguity of the element-wise division based searching function also relates to the array geometry. Moreover, we have the following result.

Theorem 2: For an M-element ($M \geq 3$) array, assume that there exist four sensors labeled as a, b, c, d (two of these four sensors could be a same sensor) satisfying the following three conditions.

1) The distance between sensor a and sensor b is no greater than $\lambda/4$.
2) The projection of the line segment $\vec{bc}$ onto the vector $\vec{ab}$ is no greater than $\lambda/4$.
3) The vector $\vec{bc}$ is not parallel to $\vec{ab}$, i.e., $\vec{bc} \nparallel \vec{ab}$.

Then, for two distinct DOAs θ_p and θ_q, there is only one specific point (θ_p', θ_q') satisfying $(\theta_p', \theta_q') \neq (\theta_p, \theta_q)$ and $\theta_p', \theta_q' \in [-180°, 180°)$ such that

$$\mathbf{a}^*(\theta_p) \odot \mathbf{a}(\theta_q) = \mathbf{a}^*(\theta_p') \odot \mathbf{a}(\theta_q').$$

The ambiguous point (θ_p', θ_q') is given by

$$\theta_p' = \begin{cases} \theta_q + \pi, & \theta_q \leq 0, \\ \theta_q - \pi, & \theta_q > 0, \end{cases} \quad \theta_q' = \begin{cases} \theta_p + \pi, & \theta_p \leq 0, \\ \theta_p - \pi, & \theta_p > 0. \end{cases} \qquad (23)$$

Proof: See Appendix B. ∎

Theorem 2 implies that the proposed DOA estimator is unambiguous when the array satisfies the conditions listed in Theorem 2 and the DOAs are confined in $[-90°, 90°]$.

When the DOAs are not confined in $[-90°, 90°]$ or there is no prior information on the DOAs, we only need to find the $K - 1$ largest peaks of $f'(\theta, \varphi)$ with distinct values, since $f(\theta_k, \theta_1) = f(\theta_k', \theta_1')$ holds, in which (θ_k', θ_1') denotes the ambiguous point corresponding to (θ_k, θ_1). The associated DOAs can be calculated by (23). Meanwhile, if one of the DOAs is roughly known, all the DOAs can be easily identified.

Suppose that the estimated DOA groups are $(\bar{\theta}_k, \bar{\varphi}_k)$, $(k = 1, 2, \ldots, 2K - 2)$. Notice that $K - 1$ elements of $\{\bar{\varphi}_k\}$ are equal to θ_1 under the ideal case. Hence, when $K > 2$, the true DOA groups can be identified as

$$\{\hat{i}_1, \ldots, \hat{i}_{K-1}\} = \arg \min_{\{i_k\} \subset S_K} \mathrm{var}\left(\bar{\varphi}_{i_1}, \ldots, \bar{\varphi}_{i_{K-1}}\right), \qquad (24)$$

where the set $S_K = \{1, 2, \ldots, 2K - 2\}$ and $\mathrm{var}(\cdot)$ denotes the variance. And then, the final DOA estimates are given by

$$\hat{\theta}_1 = \frac{1}{K-1} \sum_{k=1}^{K-1} \bar{\varphi}_{\hat{i}_k}, \quad \hat{\theta}_k = \bar{\varphi}_{\hat{i}_k}, \ k = 2, 3, \ldots, K. \qquad (25)$$

With the estimated DOAs and (19), the gain-phase vector is given by

$$\hat{\mathbf{g}} = \frac{1}{a_1(\hat{\theta}_1)\hat{b}_{1,1}} \mathbf{D}^{-1}(\mathbf{a}(\hat{\theta}_1))\hat{\mathbf{b}}_1, \qquad (26)$$

where $a_1(\hat{\theta}_1)$ and $\hat{b}_{1,1}$ denote the 1st elements of $\mathbf{a}(\hat{\theta}_1)$ and $\hat{\mathbf{b}}_1$, respectively. Based on $\hat{\mathbf{g}}$, the sensor gains and phases can be straightforwardly obtained as $\hat{\rho}_m = |\hat{g}_m|$, $\hat{\phi}_m = \angle(\hat{g}_m)$, $m = 2, 3, \ldots, M$.

Based on $\{\hat{v}_k\}$, the noncircular phases can also be estimated as

$$\hat{\alpha}_k = -\angle(\hat{v}_k/\hat{g}_M^*), \quad k = 1, 2, \ldots, K. \qquad (27)$$

Remark 2: The problem of DOA ambiguity can be solved by (24) when $K > 2$. For the case that $K = 2$, in order to avoid DOA ambiguity, the DOAs need to be confined in $[-90°, 90°]$ or at least one of the DOAs is roughly known. Nevertheless, the algorithm for estimating the spatial signatures provided in Section III-A has no such limitation and applies to arbitrary CSA. Meanwhile, for some special array geometries, e.g, URA and regular-hexagonal shaped ESPAR (electronically steerable parasitic antenna radiator) array [32], an ESPRIT-like algorithm could be designed by investigating the shift-invariance structure.

IV. STOCHASTIC CRAMÉR-RAO BOUND

In this section, we derive the stochastic CRB, which is relevant to the considered problem in this paper.

Based on the stochastic assumption, the likelihood function of the augmented array output $\bar{\mathbf{y}}(t)$ is given by [27]

$$p(\bar{\mathbf{y}}(t)|\boldsymbol{\mu}_a) = \pi^{-M} \left[\det(\mathbf{R}_{\bar{y}})\right]^{-\frac{1}{2}} \exp\left(-\frac{1}{2}\bar{\mathbf{y}}^H(t)\mathbf{R}_{\bar{y}}^{-1}\bar{\mathbf{y}}(t)\right),$$

where the vector $\boldsymbol{\mu}_a$ consisting of all the unknown real parameters can be expressed as

$$\boldsymbol{\mu}_a = [\boldsymbol{\mu}^T, \mathbf{p}^T, \sigma_n^2]^T \qquad (28)$$

with

$$\boldsymbol{\mu} = [\rho_2, \rho_3, \ldots, \rho_M, \phi_2, \phi_3, \ldots, \phi_M, \boldsymbol{\theta}^T, \boldsymbol{\alpha}^T]^T \quad (29)$$

and $\mathbf{p} \in \mathbb{R}^{K(K-1)/2 \times 1}$ consisting of all the unknown elements of the real symmetric matrix $\mathbf{R}_s$.

Ignoring the constant term, the log-likelihood function of T snapshots is given by

$$L(\boldsymbol{\mu}_a) = -\prod_{t=1}^{T} p(\bar{\mathbf{y}}(t)|\boldsymbol{\mu}_a)$$
$$= \frac{T}{2} \left(\ln \left(\det(\mathbf{R}_{\bar{y}}) \right) + \mathrm{Tr}(\mathbf{R}_{\bar{y}}^{-1} \hat{\mathbf{R}}_{\bar{y}}) \right). \quad (30)$$

The log-likelihood function concentrated with respect to the parameters of $\mathbf{p}$ and σ_n^2 is given by [1]

$$\bar{L}(\boldsymbol{\mu}) = \frac{T}{2} \ln \left(\det(\bar{\mathbf{B}} \hat{\mathbf{R}}_s \bar{\mathbf{B}}^H + \hat{\sigma}_n^2 \mathbf{I}_{2M}) \right), \quad (31)$$

where $\hat{\sigma}_n^2 = \mathrm{Tr}(\mathbf{P}_{\bar{\mathbf{B}}}^{\perp} \hat{\mathbf{R}}_{\bar{y}})/(2M - K)$ and $\hat{\mathbf{R}}_s = \bar{\mathbf{B}}^{\dagger} \hat{\mathbf{R}}_{\bar{y}} \bar{\mathbf{B}}^{\dagger H} - \hat{\sigma}_n^2(\bar{\mathbf{B}}^H \bar{\mathbf{B}})^{-1}$ with $\mathbf{P}_{\bar{\mathbf{B}}}^{\perp} = \mathbf{I}_{2M} - \bar{\mathbf{B}} \bar{\mathbf{B}}^{\dagger}$. The stochastic ML estimate of $\boldsymbol{\mu}$ is obtained by minimizing the log-likelihood function $\bar{L}(\boldsymbol{\mu})$ with respect to the elements of $\boldsymbol{\mu}$.

Other than directly deriving the Fisher information matrix, the stochastic CRB can also be obtained by deriving the asymptotic covariance matrix of the corresponding stochastic ML estimator, since the stochastic ML method can asymptotically achieve the stochastic CRB (see [33, Th. 3]). Moreover, we have the following theorem [34, Th. 1].

Theorem 3: The stochastic CRB for the parameters of $\boldsymbol{\mu}$ satisfies

$$[\overline{\mathrm{CRB}}(\boldsymbol{\mu})]^{-1} = \lim_{T \to \infty} \frac{\partial^2 F(\boldsymbol{\mu})}{\partial \boldsymbol{\mu} \partial \boldsymbol{\mu}^T} \quad (32)$$

where $\overline{\mathrm{CRB}}(\boldsymbol{\mu})$ is the stochastic CRB for a single snapshot and $F(\boldsymbol{\mu}) = \bar{L}(\boldsymbol{\mu})/T$ is the average concentrated log-likelihood function.

Let $\mathbf{F}''(\boldsymbol{\mu})$ be the Hessian matrix of $F(\boldsymbol{\mu})$ and $\mathbf{F}_0''(\boldsymbol{\mu}) = \lim_{T \to \infty} \mathbf{F}''(\boldsymbol{\mu})$. Following along the lines of the derivation given in [35], we get

$$[\mathbf{F}_0''(\boldsymbol{\mu})]_{pq} = \sigma_n^{-2} \Re \left(\mathrm{Tr} \left(\mathbf{U} \frac{\partial \bar{\mathbf{B}}^H}{\partial \mu_q} \mathbf{P}_{\bar{\mathbf{B}}}^{\perp} \frac{\partial \bar{\mathbf{B}}}{\partial \mu_p} \right) \right), \quad (33)$$

where

$$\mathbf{U} = \mathbf{R}_s \bar{\mathbf{B}}^H \mathbf{R}_{\bar{y}}^{-1} \bar{\mathbf{B}} \mathbf{R}_s = \sigma_n^{-2} \mathbf{R}_s \bar{\mathbf{B}}^H \bar{\mathbf{B}}$$
$$\cdot \left(\mathbf{I}_{2M} - \sigma_n^{-2}(\mathbf{R}_s^{-1} + \sigma_n^{-2} \bar{\mathbf{B}}^H \bar{\mathbf{B}})^{-1} \bar{\mathbf{B}}^H \bar{\mathbf{B}} \right) \mathbf{R}_s. \quad (34)$$

Notice that $\bar{\mathbf{B}}^H \bar{\mathbf{B}} = \mathbf{B}_1^H \mathbf{B}_1 + \mathbf{B}_2^H \mathbf{B}_2 = 2 \Re(\mathbf{B}_1^H \mathbf{B}_1)$. It follows that $\mathbf{U} \in \mathbb{R}^{K \times K}$.

One can easily obtain $\mathbf{F}_0''(\boldsymbol{\mu})$ by deriving the partial derivatives in (33). A simplified expression of $\mathbf{F}_0''(\boldsymbol{\mu})$ is derived in Appendix C and expressed as

$$\mathbf{F}_0''(\boldsymbol{\mu}) = \sigma_n^{-2} \Re \left(\mathbf{J} \begin{bmatrix} \mathbf{F}_{gg} & \mathbf{F}_{gs} \\ \mathbf{F}_{gs}^H & \mathbf{F}_{ss} \end{bmatrix} \mathbf{J}^T \right), \quad (35)$$

where $\mathbf{J} = \mathrm{blkdiag}(\mathbf{J}_0, \mathbf{J}_0, \mathbf{I}_{2K})$ with $\mathbf{J}_0 = [\mathbf{0}, \mathbf{I}_{M-1}] \in \mathbb{R}^{(M-1) \times M}$. In (35), the gain-phase errors block

$$\mathbf{F}_{gg} = 2(\mathbf{H}_g^H \mathbf{U} \mathbf{H}_g) \odot (\mathbf{1}_{2,2} \otimes \boldsymbol{\Xi}_1^T)$$
$$+ 2(\mathbf{H}_g^H \mathbf{U} \mathbf{H}_g^*) \odot (\mathbf{1}_{2,2} \otimes (\boldsymbol{\Gamma} \boldsymbol{\Xi}_2)^T), \quad (36)$$

where $\boldsymbol{\Xi}_1, \boldsymbol{\Xi}_2 \ (\in \mathbb{C}^{M \times M})$ satisfy $\mathbf{P}_{\bar{\mathbf{B}}}^{\perp} = \begin{bmatrix} \boldsymbol{\Xi}_1 & \boldsymbol{\Xi}_2^H \\ \boldsymbol{\Xi}_2 & (\boldsymbol{\Gamma} \boldsymbol{\Xi}_1 \boldsymbol{\Gamma})^* \end{bmatrix}$, and

$$\mathbf{H}_g = [\mathbf{H}_\rho, \mathbf{H}_\phi] = [(\mathbf{D}(\exp(j\boldsymbol{\phi})) \mathbf{A} \mathbf{D}(\boldsymbol{\beta}))^H, -j\mathbf{B}_1^H]. \quad (37)$$

The block containing the parameters of the source signals, i.e., $\boldsymbol{\theta}$ and $\boldsymbol{\alpha}$, is given by

$$\mathbf{F}_{ss} = (\mathbf{1}_{2,2} \otimes \mathbf{U}) \odot (\mathbf{H}_s^H \mathbf{P}_{\bar{\mathbf{B}}}^{\perp} \mathbf{H}_s)^T, \quad (38)$$

where

$$\mathbf{H}_s = [\mathbf{H}_\theta, \mathbf{H}_\alpha] = \begin{bmatrix} \mathbf{D}(\mathbf{g}) \boldsymbol{\Lambda} \mathbf{D}(\boldsymbol{\beta}) & j\frac{1}{2}\mathbf{B}_1 \\ \mathbf{D}^*(\boldsymbol{\Gamma} \mathbf{g}) \boldsymbol{\Lambda} \mathbf{D}^*(\boldsymbol{\beta}) & -j\frac{1}{2}\mathbf{B}_2 \end{bmatrix}, \quad (39)$$

with $\boldsymbol{\Lambda} = [\partial \mathbf{a}(\theta_1)/\partial \theta_1, \ldots, \partial \mathbf{a}(\theta_K)/\partial \theta_K]$. The cross term

$$\mathbf{F}_{gs} = (\mathbf{H}_g^H (\mathbf{1}_{1,2} \otimes \mathbf{U})) \odot ((\mathbf{1}_{2,1} \otimes \boldsymbol{\Xi}_3^T) \mathbf{H}_s^*)$$
$$+ (\mathbf{H}_g^T (\mathbf{1}_{1,2} \otimes \mathbf{U})) \odot ((\mathbf{1}_{2,1} \otimes (\boldsymbol{\Gamma} \boldsymbol{\Xi}_4^T)) \mathbf{H}_s^*), \quad (40)$$

where $\boldsymbol{\Xi}_3, \boldsymbol{\Xi}_4 \ (\in \mathbb{C}^{2M \times M})$ satisfy $\mathbf{P}_{\bar{\mathbf{B}}}^{\perp} = [\boldsymbol{\Xi}_3, \boldsymbol{\Xi}_4]$.

The stochastic CRB follows from (32) and (35) that

$$\mathrm{CRB}(\boldsymbol{\mu}) = \frac{1}{T} [\mathbf{F}_0''(\boldsymbol{\mu})]^{-1}$$
$$= \frac{\sigma_n^2}{T} \left[\Re \left(\mathbf{J} \begin{bmatrix} \mathbf{F}_{gg} & \mathbf{F}_{gs} \\ \mathbf{F}_{gs}^H & \mathbf{F}_{ss} \end{bmatrix} \mathbf{J}^T \right) \right]^{-1}. \quad (41)$$

For the stochastic CRB, we have the following meaningful property.

Property 1: The stochastic CRB is independent of the sensor phases.

Proof: To prove this property, it suffices to show that the (p, q)th element of $\mathrm{CRB}(\boldsymbol{\mu})$ or the (p, q)th element of $\mathbf{F}_0''(\boldsymbol{\mu})$ is independent of $\boldsymbol{\phi}$ for arbitrary p, q.

By definition, $\bar{\mathbf{B}}$ can be rewritten as $\bar{\mathbf{B}} = \mathbf{D}(\bar{\boldsymbol{\phi}}) \bar{\mathbf{B}}'$, where $\bar{\boldsymbol{\phi}} = [\exp(j\boldsymbol{\phi}^T), \exp(-j(\boldsymbol{\Gamma} \boldsymbol{\phi})^T)]^T$ and

$$\bar{\mathbf{B}}' = \mathbf{D}(\bar{\boldsymbol{\phi}}^*) \bar{\mathbf{B}} = \begin{bmatrix} \mathbf{D}(\boldsymbol{\rho}) \mathbf{A} \mathbf{D}(\boldsymbol{\beta})) \\ \mathbf{D}(\boldsymbol{\Gamma} \boldsymbol{\rho}) \mathbf{A} \mathbf{D}(\boldsymbol{\beta}^*)) \end{bmatrix},$$

It follows that $\bar{\mathbf{B}}^H \bar{\mathbf{B}} = \bar{\mathbf{B}}'^H \bar{\mathbf{B}}'$ and $\mathbf{P}_{\bar{\mathbf{B}}}^{\perp} = \mathbf{D}(\bar{\boldsymbol{\phi}}) \mathbf{P}_{\bar{\mathbf{B}}'}^{\perp} \mathbf{D}(\bar{\boldsymbol{\phi}}^*)$. Obviously, the matrices $\bar{\mathbf{B}}^H \bar{\mathbf{B}}$, $\mathbf{P}_{\bar{\mathbf{B}}'}^{\perp}$ and $\mathbf{U}$ (see (34)) are independent of $\boldsymbol{\phi}$. Moreover, from (56) and (57), $\partial \bar{\mathbf{B}}/\partial \mu_p$ can always be written as the matrix product of $\mathbf{D}(\bar{\boldsymbol{\phi}})$ and a matrix that is independent of $\boldsymbol{\phi}$. Based on the above discussion, it can be easily verified that the (p, q)th element of $\mathbf{F}_0''(\boldsymbol{\mu})$ shown in (33) is independent of $\boldsymbol{\phi}$ for arbitrary p and q, which completes the proof. ∎

V. SIMULATIONS

In this section, the performance of the proposed method is evaluated in comparison with two representative methods, including the WF method [12] and the CY method [16]. Meanwhile, the stochastic CRB for circular Gaussian signals[2]

---

[1] The scaling factor T, which is independent of $\boldsymbol{\mu}$, is usually ignored in the literature.

[2] In [36], the CRB without concentrated with respect to the nuisance parameters of the source covariance matrix and the noise power is obtained by directly deriving the blocks of the Fisher information matrix. A closed-form expression is still not available in the literature. However, it can be easily obtained by using Theorem 3. The specific expression is omitted in this paper.
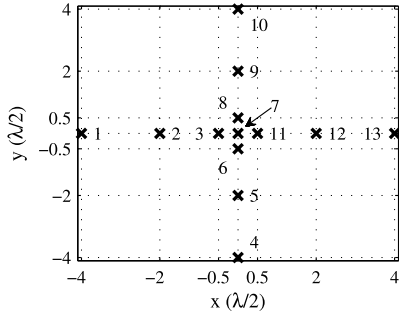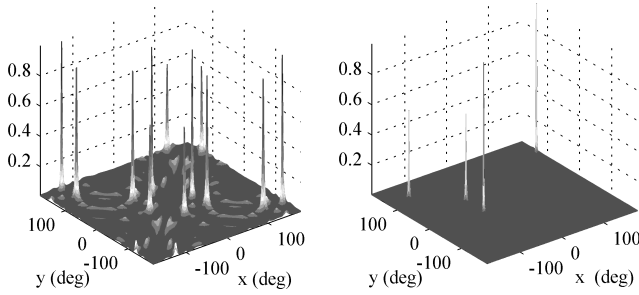
Fig. 1. Array configuration and antenna indexes.

Fig. 2. Left: Normalized two-dimensional spectrum of the CY method. Right: Normalized two-dimensional spectrum of $f(y, x)$. First experiment.
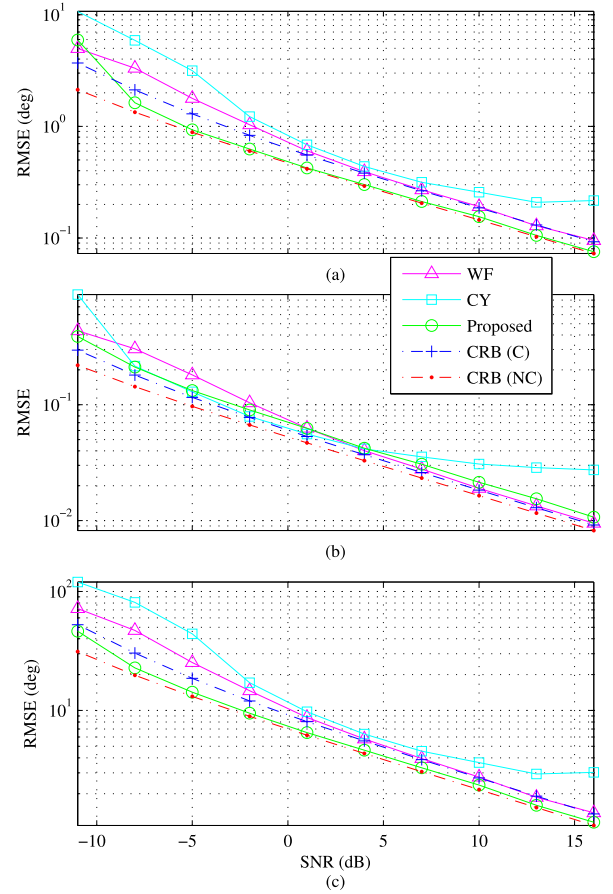

Fig. 3. Estimation performance for two SSNC sources with small sensor phase errors. (a) RMSE of DOA estimation versus SNR. (b) RMSE of sensor gain errors estimation versus SNR. (c) RMSE of sensor phase errors estimation 2 versus SNR. Second experiment.

and the stochastic CRB for SSNC signals are also listed for comparison.

In the simulations, a 13-element CSA composed of two identical linear arrays is employed as shown in Fig. 1. Clearly, there exist three antennas, such as the antennas 3, 6 and 7, satisfying the conditions in Theorem 2. The powers of the signals are set to be a same value. Except for the fourth experiment in section V-C, the signals are independently drawn from complex Gaussian distribution such that they are uncorrelated with each other. In each experiment, 1000 independent Monte Carlo runs are used to obtain the curves. The sensor gains and phases are defined as

$$\mathbf{g} = \mathbf{1}_M + [1, \Delta\mathbf{g}^T]^T, \quad \boldsymbol{\phi} = [0, \Delta\boldsymbol{\phi}^T]^T,$$

where $\Delta\mathbf{g}$ and $\Delta\boldsymbol{\phi}$ are the sensor gain errors and phase errors, respectively. Unless otherwise specified, the elements of $\Delta\boldsymbol{\rho}$ and $\Delta\boldsymbol{\phi}$ are drawn from uniform distribution with the intervals $[-0.15, 0.15]$ and $[-180°, 180°]$, respectively.

A. Example of Two-Dimensional Spectra

In the first experiment, we set $\boldsymbol{\theta} = [-58° \ -10° \ 45°]^T$, $\boldsymbol{\alpha} = [-20° \ 70° \ 60°]^T$, $T = 200$, $\boldsymbol{\rho} = [1 \ 1.11 \ 0.89 \ 0.92$ $0.91 \ 1.07 \ 0.85 \ 0.94 \ 1.14 \ 1.12 \ 1.02 \ 0.86 \ 0.95]^T$ and $\boldsymbol{\phi} =$ $[0 \ 0.03 \ 2.46 \ -1.18 \ -2.69 \ 2.37 \ 1.13 \ 1.70 \ -2.72 \ -1.99 \ -0.47$ $-2.32 \ -1.90]^T$. The signal to noise ratio (SNR) is set to be 5 dB. The searching grid is set to $1°$. The normalized two-dimensional spectra of the CY method and the function $f(y, x)$ are shown in Fig. 2.

The coordinates of the four largest peaks in the right figure of Fig. 2 are $(10°, -58°)$, $(45°, -58°)$, $(122°, 170°)$ and $(122°, -135°)$, which satisfy the relationship in (23). Meanwhile, there are only two strong peaks in the range $[-90°, 90°]$ of both the x and y axes. The left figure of Fig. 2 contains $12 (= 2K(K-1))$ obvious peaks (the corresponding coordinates are omitted here). Obviously, it is very hard to identify all the peaks for the CY method, especially when the number of sources K gets larger.

B. Different SNR

The second experiment investigates the performance of the proposed method for two SSNC sources with small phase errors. We set $\boldsymbol{\theta} = [-8.04°, 20.12°]^T$, $\boldsymbol{\alpha} = [-20°, 70°]^T$ and $T = 200$. The entries of the phase errors $\Delta\boldsymbol{\phi}$ are independently drawn from the uniform distribution over the interval $[-20°, 20°]$. The SNR is varied from -11 dB to 16 dB in steps of 3 dB. The statistical results for the parameters of DOAs, sensor gain and phase errors are shown in Fig. 3.

It shows that the CRB for SSNC signals is strictly lower than the CRB for circular signals. The root mean square error (RMSE) curves of the WF method for all the three parameters can closely approach the circular Gaussian CRB when SNR > 0 dB. However, it is inferior to the proposed method for estimating the parameters of DOA and sensor
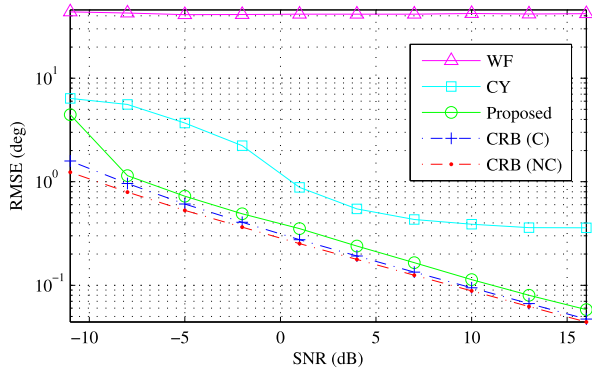
Fig. 4. Estimation performance for three SSNC sources with large sensor phase errors: RMSE of DOA estimation versus SNR. Third experiment.

Fig. 5. RMSE of DOA estimation versus correlation coefficient. Fourth experiment.

phase errors. For these two parameters, the proposed method has the best estimation performance, and the corresponding RMSEs can closely approach the associated CRBs, respectively, when SNR > -5 dB. For the sensor gain errors, the proposed method is somewhat inferior to the WF method at high SNR, but outperforms the WF method at low SNR.

The third experiment investigates the performance of the proposed method for three SSNC sources with large sensor phase errors. We set $\boldsymbol{\theta} = [-8°, 20°, 45°]^T$, $\boldsymbol{\alpha} = [-20°,\ 70°,\ 80°]^T$, $T = 200$ and the SNR is varied from -11 dB to 16 dB in steps of 3 dB. The statistical results are shown in Fig. 4. It is shown that the WF method is completely failed to estimate the DOAs. The other two methods are capable of providing a successful DOA estimation with different performance, and the proposed method significantly outperforms the CY method. Although the RMSE of the proposed is greater than the CRB, there is only a small gap between them.

C. Different Correlation of Sources

The fourth experiment investigates the performance of the proposed method for different correlation coefficients. The parameters of DOAs, noncircular phases and the number of snapshots are set as the second experiment in Section V-B. The SNR is fixed to be 5 dB. Let ϵ denote the correlation coefficient between $\bar{s}_1(t)$ and $\bar{s}_2(t)$. The signals are generated as

$$\bar{s}_1(t) = \sin((\arcsin \epsilon)/2)\bar{s}_1'(t) + \cos((\arcsin \epsilon)/2)\bar{s}_2'(t),$$
$$\bar{s}_2(t) = \cos((\arcsin \epsilon)/2)\bar{s}_1'(t) + \sin((\arcsin \epsilon)/2)\bar{s}_2'(t),$$

where $\bar{s}_1'(t)$ and $\bar{s}_2'(t)$ are independently drawn from Gaussian distribution with mean zero and the variance calculated by the corresponding SNR. It can be easily verified that the correlation coefficient between $\bar{s}_1(t)$ and $\bar{s}_2(t)$ is ϵ. In the simulation, ϵ is varied from 0 to 0.99. The statistical results are shown in Fig. 5.

The simulation results show that the proposed method significantly outperforms the CY method, while the WF method is completely failed to estimate the DOAs even when the sources are uncorrelated. Fig. 5 demonstrates that the proposed method agrees well with the CRB for SSNC signals when $\epsilon \leq 0.9$. However, increasing the correlation
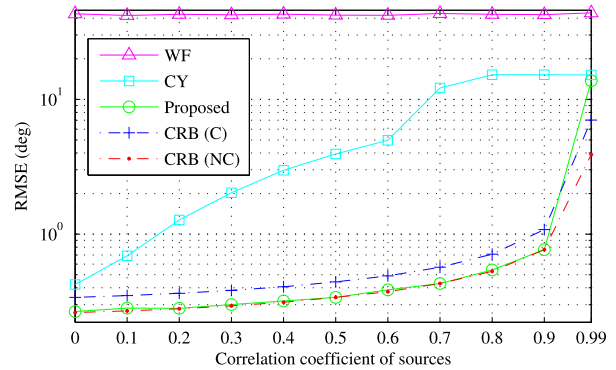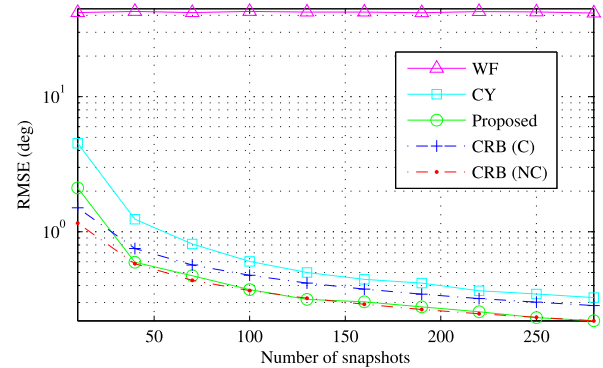

Fig. 6. RMSE of DOA estimation versus the number of snapshots. Fifth experiment.

coefficient of sources causes a dramatic increase of the RMSE of the CY method. It is seen that the RMSE of the proposed method is less than $1°$ even when $\epsilon = 0.9$. As a comparison, the CY method is completely failed when $\epsilon > 0.6$. Meanwhile, it also indicates that all the methods fail to cope with the highly correlated case when $\epsilon = 0.99$, and the CRB itself is getting very large in this case.

D. Different Number of Snapshots

The fifth experiment investigates the performance of the proposed method for different number of snapshots. The parameters are the same as those of the second experiment in Section V-B except that SNR = 5 dB and the number of snapshots is varied from 10 to 280 in steps of 30. The statistical results are shown in Fig. 6.

It is seen from Fig. 6 that the proposed method outperforms all the other two methods and closely approaches the CRB for SSNC signals when $T > 40$. However, the CY method cannot approach the corresponding CRB and the WF method fails to estimate the DOAs.

E. Different Noncircular Phase

The sixth experiment investigates the performance of the proposed method for different noncircular phases. We set $\boldsymbol{\theta} = [-8°, 20°]^T$, $T = 200$ and SNR = 5 dB. The noncircular phases are set to $0°$ and $0° + \Delta\alpha$, respectively, where $\Delta\alpha$ is varied from $0°$ to $360°$ in steps of $20°$. The statistical results are shown in Fig. 7.
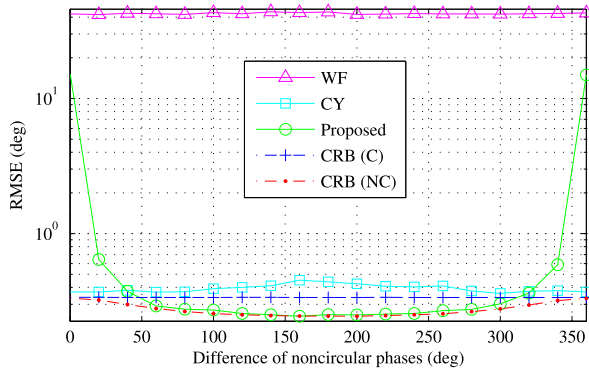
Fig. 7. RMSE of DOA estimation versus the difference of noncircular phases. Sixth experiment.
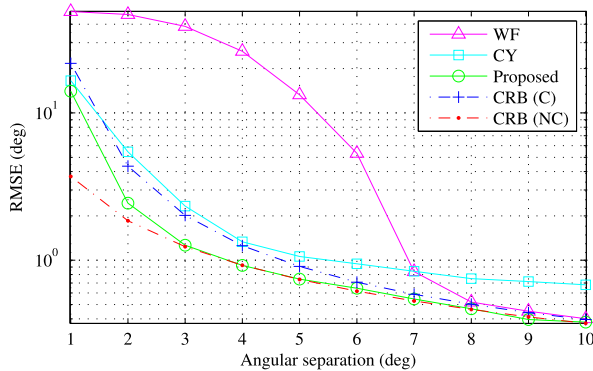

Fig. 8. RMSE of DOA estimation versus angular separation. Seventh experiment.

Fig. 9. RMSE of DOA estimation versus the standard derivation of sensor phase errors. Eighth experiment.

The results demonstrate the following conclusions. First, the CRB for circular sources is insensitive to the difference of noncircular phases. Second, compared to the CRB for circular signals, the CRB for SSNC signals can achieve significant performance gain when $\exp(j\alpha') \neq 1$, and the largest performance gain is achieved when $\alpha' = 180°$. Third, the proposed method has the best performance, and closely approaches the CRB for SSNC signals when the phase difference is large enough. In addition, Fig. 7 also shows that the performance of the CY method is slightly affected by the difference of the noncircular phases. However, the theoretic analysis of this phenomenon is beyond the scope of this paper.

F. Different Angular Separation

The seventh experiment studies the RMSE performance versus angular separation. We set $\boldsymbol{\theta} = [0°, 0° + \Delta\theta]^T$, $\boldsymbol{\alpha} = [-42°, 67°]^T$, $T = 200$ and SNR = 10 dB. The entries of the phase errors $\Delta\boldsymbol{\phi}$ are independently drawn from the uniform distribution over the interval $[-20°, 20°]$. The angular separation $\Delta\theta$ is varied from $1°$ to $10°$. Fig. 8 demonstrates that the proposed method outperforms the other two competitors, and closely approaches the CRB for SSNC signals when the angular separation between two sources is no less than $3°$. It also shows that the CRB for SSNC signals is less than the CRB for circular signals especially when the angular separation is small.

G. Different Sensor Phase Errors

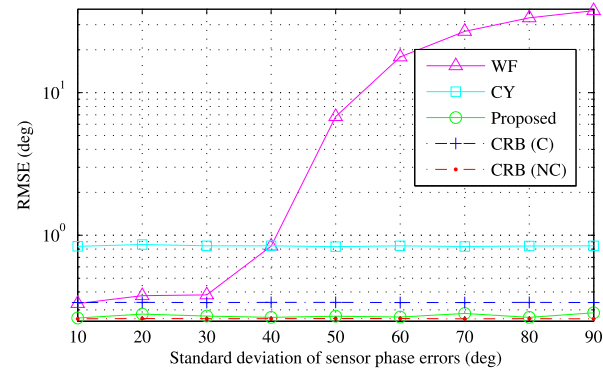The eighth experiment studies the RMSE performance versus the standard derivation of sensor phase errors.

The parameters are the same as those in Section V-F except that SNR = 5 dB, $\boldsymbol{\theta} = [-8°, 20°]^T$ and the sensor phase errors are set to be $\phi_m = \sqrt{12}\sigma_\phi\kappa_m, m = 2, 3, \ldots, M$, where $\{\kappa_m\}$ are independently drawn from uniform distribution over the interval $[-0.5, 0.5]$, and the standard derivation σ_ϕ is varied from $10°$ to $90°$. It is seen from Fig. 9 that both the two CRBs, the CY method and the proposed method are independent of the phase errors. The proposed method has the best estimation performance, and closely approaches the CRB for SSNC signals. The WF method outperforms the CY method and closely approaches the CRB when $\sigma_\phi \leq 30°$, but it is inferior to the CY method when $\sigma_\phi > 40°$.

VI. CONCLUSION

In this paper, a two steps method is proposed for the problem of jointly estimating the parameters of DOAs and gain-phase errors for noncircular sources with CSA. Different from the existing methods, the proposed auto-calibration method first estimates the spatial signatures, based on which the estimation algorithm for the parameters of DOAs and the gain-phase errors is derived. This strategy brings a number of advantages in comparison with the existing techniques, such as applicable to incoherent sources, applicable to large gain-phase errors and acceptable computational complexity. Meanwhile, the proposed method is capable of providing 360° azimuthal coverage when $K > 2$ or at least one of the DOAs is roughly known. The corresponding stochastic CRB is derived as well. Simulation results show that the proposed method outperforms the conventional methods especially when the differences of the noncircular phases are large.

APPENDIX A
PROOF OF THEOREM 1

Clearly, $\mathbf{G}$ is positive semidefinite. To prove Theorem 1, it suffices to show that $\mathbf{x}^H\mathbf{G}\mathbf{x} > 0$ for all $\mathbf{x} \in S_x$, where $S_x = \{\mathbf{x}|\mathbf{x} \in \mathbb{C}^{M \times 1}, \mathbf{x} \nparallel (\mathbf{1}_{M,1} \oslash \bar{\mathbf{g}}), \mathbf{x} \neq \mathbf{0}\}$. Since

$$\mathbf{x}^H\mathbf{G}\mathbf{x} = \|\mathbf{P}_{\mathbf{U}_{s1}}^{\perp}\mathbf{D}(\mathbf{x})\mathbf{U}_{s2}\|^2$$
$$= \|g_0\mathbf{P}_{\mathbf{B}}^{\perp}\mathbf{D}(\mathbf{x} \odot \bar{\mathbf{g}})\mathbf{B}\mathbf{D}(\boldsymbol{\beta}^*)\mathbf{T}^{-1}\|^2, \quad (42)$$

we only need to show that $\mathbf{P}_{\mathbf{B}}^{\perp}\mathbf{D}(\mathbf{x} \odot \bar{\mathbf{g}})\mathbf{B} \neq \mathbf{0}$ for all $\mathbf{x} \in S_x$, or equivalently, $\text{span}(\mathbf{D}(\bar{\mathbf{x}})\mathbf{B}) \neq \text{span}(\mathbf{B})$ for any $\bar{\mathbf{x}} = \mathbf{x} \odot \bar{\mathbf{g}} \neq \mathbf{1}_{M,1}$.

If there exists an $\mathbf{x} \in S_x$ making span$(\mathbf{B}) =$ span$(\mathbf{D}(\mathbf{x} \odot \bar{\mathbf{g}})\mathbf{B})$. There must exist a unique nonsingular matrix $\bar{\mathbf{T}} \in \mathbb{C}^{K \times K}$ such that

$$\mathbf{D}(\mathbf{x} \odot \bar{\mathbf{g}})\mathbf{B} = \mathbf{B}\bar{\mathbf{T}}.$$
$$\Rightarrow (\mathbf{B}^T \circ \mathbf{I}_M)(\mathbf{x} \odot \bar{\mathbf{g}}) = (\mathbf{I}_K \circ \mathbf{B})\,\text{vec}(\bar{\mathbf{T}})$$
$$\Rightarrow \boldsymbol{\Upsilon}\dot{\mathbf{x}} = \mathbf{0}, \tag{43}$$

where vec$(\cdot)$ and $\circ$ denote the vector operator and column-wise Kronecker product, respectively, $\dot{\mathbf{x}} = [\bar{\mathbf{x}}^T, \bar{\mathbf{t}}^T]^T$ with $\bar{\mathbf{t}} = \text{vec}(\bar{\mathbf{T}})$, $\boldsymbol{\Upsilon} = [\boldsymbol{\Upsilon}_1, \boldsymbol{\Upsilon}_2] \in \mathbb{C}^{MK \times (M+K^2)}$ with

$$\boldsymbol{\Upsilon}_1 = \begin{bmatrix} \mathbf{D}(\mathbf{b}_1) \\ \mathbf{D}(\mathbf{b}_2) \\ \vdots \\ \mathbf{D}(\mathbf{b}_K) \end{bmatrix}, \quad \boldsymbol{\Upsilon}_2 = \begin{bmatrix} \mathbf{B} & & & \\ & \mathbf{B} & & \\ & & \ddots & \\ & & & \mathbf{B} \end{bmatrix},$$

As $\dot{\mathbf{x}} = [\mathbf{1}_{M,1}^T, \text{vec}(\mathbf{I}_M)^T]^T$ is a solution of (43), we only need to show that

$$\text{rank}(\boldsymbol{\Upsilon}) = M + K^2 - 1. \tag{44}$$

Note that $M + K^2 - 1 - MK = (K + 1 - M)(K - 1) \leq 0$, i.e., $M + K^2 - 1 \leq MK$, when $0 < K < M$.

When $M = K + 1$, $\boldsymbol{\Upsilon}$ has the size $(K^2 + K) \times (K^2 + K + 1)$. If $\boldsymbol{\Upsilon}$ is not of full row rank, there exists a nonzero vector $\ddot{\mathbf{x}} = [\ddot{\mathbf{x}}_1^T, \ddot{\mathbf{x}}_2^T, \ldots, \ddot{\mathbf{x}}_K^T]^T$ with $\ddot{\mathbf{x}}_k \in \mathbb{C}^{M \times 1}$ $(k = 1, 2, \ldots, K)$ such that $\ddot{\mathbf{x}}^H \boldsymbol{\Upsilon} = \mathbf{0}$, which is equivalent to

$$\left[\sum_{k=1}^{K} \ddot{\mathbf{x}}_k^H \odot \mathbf{b}_k^T, \ddot{\mathbf{x}}_1^H \mathbf{B}, \ddot{\mathbf{x}}_2^H \mathbf{B}, \ldots, \ddot{\mathbf{x}}_K^H \mathbf{B} \right] = \mathbf{0}. \tag{45}$$

Since $\mathbf{B} \in \mathbb{C}^{M \times (M-1)}$ and the array is ambiguous, we have $\dim(\text{null}(\mathbf{B}^H)) = 1$. The $(k+1)$th $(k \in \{1, 2, \ldots, K\})$ term in (45) implies that $\ddot{\mathbf{x}}_k = \mathbf{0}$ or $\ddot{\mathbf{x}}_k \parallel \ddot{\mathbf{x}}_0$, where $\ddot{\mathbf{x}}_0$ satisfies span$(\ddot{\mathbf{x}}_0) = \text{null}(\mathbf{B}^H)$. Thus, we can write $\ddot{\mathbf{x}}_k = x_k' \ddot{\mathbf{x}}_0$. And then the first term in (45) can be rewritten as

$$\mathbf{1}_{K,1}^T \mathbf{D}(\mathbf{x}_0'^*)\mathbf{B}^T \mathbf{D}(\ddot{\mathbf{x}}_0^*) = \mathbf{x}_0'^H \mathbf{B}^T \mathbf{D}(\ddot{\mathbf{x}}_0^*) = \mathbf{0}, \tag{46}$$

where $\mathbf{x}_0' = [x_1', x_2', \ldots, x_K']^T$. It should be noted that $\ddot{\mathbf{x}}_0$ has at most one zero element, otherwise, $\mathbf{B}$ is not of full column rank. Consequently, $\mathbf{B}^T \mathbf{D}(\ddot{\mathbf{x}}_0^*) \in \mathbb{C}^{K \times M}$ is of full row rank. It follows that (46) cannot be hold for any nonzero vector $\mathbf{x}_0'$. Therefore, (44) holds in this case.

When $M = K + 2$, $\boldsymbol{\Upsilon}$ has the size $((M-1)K + K) \times (M - 1) + K^2 + 1)$. Based on the above discussion, there must exist a submatrix of $\boldsymbol{\Upsilon}$, denoted by $\boldsymbol{\Upsilon}_s \in \mathbb{C}^{((M-1)K \times (M-1)+K^2)}$, is of full row rank. And it can be formed with the submatrix of $\boldsymbol{\Upsilon}$ indexed by the rows and columns corresponding to $M - 1$ sensors. Using two proper permutation matrices $\mathbf{J}_L$ and $\mathbf{J}_R$, we can get

$$\boldsymbol{\Upsilon}_p = \mathbf{J}_L \boldsymbol{\Upsilon} \mathbf{J}_R = \begin{bmatrix} \boldsymbol{\Upsilon}_s & \mathbf{0} \\ \boldsymbol{\Upsilon}_{ld} & \boldsymbol{v}_{rd} \end{bmatrix}, \tag{47}$$

where $\boldsymbol{\Upsilon}_{ld} = [\mathbf{0}, \text{blkdiag}(\boldsymbol{v}_{rd}^T, \boldsymbol{v}_{rd}^T, \ldots, \boldsymbol{v}_{rd}^T)]$ with $\mathbf{0}$ having the size $K \times (M - 1)$, and $\boldsymbol{v}_{rd} = [b_{1,M}, b_{2,M}, \ldots, b_{K,M}]^T$ with $b_{k,M}$ denoting the Mth element of $\mathbf{b}_k$. Clearly,

$$\text{rank}(\boldsymbol{\Upsilon}) = \text{rank}(\boldsymbol{\Upsilon}_p) = \text{rank}(\boldsymbol{\Upsilon}_s) + \text{rank}(\boldsymbol{v}_{rd})$$
$$= (M - 1)K + 1 = M + K^2 - 1 \tag{48}$$

It follows that (44) holds.

Consider that (44) holds when $M = K + p$ $(p > 2)$. A similar proof to the case $M = K + 2$ can be provided to prove that (44) holds when $M = K + p + 1$, which completes the proof of Theorem 1.

APPENDIX B
PROOF OF THEOREM 2

For two given distinct DOAs θ_p and θ_q, assume that there exist two DOAs θ and φ satisfying $(\theta, \varphi) \neq (\theta_p, \theta_q)$ such that

$$\mathbf{a}^*(\theta_p) \odot \mathbf{a}(\theta_q) = \mathbf{a}^*(\theta) \odot \mathbf{a}(\varphi). \tag{49}$$

Without loss of generality, suppose that the sensor a and sensor b are located on the x-axis and the coordinates of the sensor a, b and c are $(x_a, 0)$, $(x_b, 0)$ and (x_c, y_c), respectively. (49) implies that

$$\exp(j\omega x_{ab}(\sin\theta_p - \sin\theta_q)) = \exp(j\omega x_{ab}(\sin\theta - \sin\varphi)) \tag{50}$$

and

$$\exp\left(j\omega(x_{cd}(\sin\theta_p - \sin\theta_q) + y_{cd}(\cos\theta_p - \cos\theta_q))\right)$$
$$= \exp\left(j\omega(x_{cd}(\sin\theta - \sin\varphi) + y_{cd}(\cos\theta - \cos\varphi))\right), \tag{51}$$

where $x_{ab} = x_a - x_b$, $x_{cd} = x_c - x_d$ and $y_{cd} = y_c - y_d$. It follows from (50) that

$$\sin\theta_p - \sin\theta_q = \sin\theta - \sin\varphi + n\lambda/x_{ab}, \tag{52}$$

where n is an integer number. Obviously, we have $|n\lambda/x_{ab}| < 4$, since θ_p and θ_q are assumed to be distinct. If the array geometry satisfies the condition 1), then we get $n = 0$.

Substitute (52) back into (51). When the sensors satisfy the condition 3), i.e., $y_{cd} \neq 0$, we get

$$\cos\theta_p - \cos\theta_q = \cos\theta - \cos\varphi + m\lambda/y_{cd}, \tag{53}$$

where m is an integer number. Based on the same analysis of n, if the array geometry satisfied the condition 2), we have $m = 0$. Then, (52) and (53) are reduced to

$$\begin{cases} \sin\theta_p - \sin\theta_q = \sin\theta - \sin\varphi \\ \cos\theta_p - \cos\theta_q = \cos\theta - \cos\varphi. \end{cases} \tag{54}$$

Let $\mathbf{r}_1 = [\sin\theta_p, \cos\theta_p]^T$, $\mathbf{r}_2 = [\sin\theta_q, \cos\theta_q]^T$, $\mathbf{r}_3 = [\sin\theta, \cos\theta]^T$ and $\mathbf{r}_4 = [\sin\varphi, \cos\varphi]^T$. (54) is equivalent to

$$\begin{cases} \mathbf{r}_1 - \mathbf{r}_2 = \mathbf{r}_3 - \mathbf{r}_4 \\ \|\mathbf{r}_3\|_2 = \|\mathbf{r}_4\|_2 = 1. \end{cases} \tag{55}$$

A geometrical explanation of (55) is shown in Fig. 10. It shows that the only solution is $\mathbf{r}_3 = -\mathbf{r}_2$ and $\mathbf{r}_4 = -\mathbf{r}_1$, which leads to the result of (23). The proof is completed.

APPENDIX C
DERIVATION OF (35)

One can easily obtain the partial derivatives in (35) as

$$\partial\bar{\mathbf{B}}/\partial\rho_p = \left[\mathbf{0}_{K,p-1}, \mathbf{h}_p^\rho, \mathbf{0}_{K,2M-2p}, \mathbf{h}_p^{\rho*}, \mathbf{0}_{K,p-1}\right]^H, \tag{56a}$$

$$\partial\bar{\mathbf{B}}/\partial\phi_p = [\mathbf{0}_{K,p-1}, \mathbf{h}_p^\phi, \mathbf{0}_{K,2M-2p}, \mathbf{h}_p^{\phi*}, \mathbf{0}_{K,p-1}]^H, \tag{56b}$$

$$\partial\bar{\mathbf{B}}/\partial\theta_p = [\mathbf{0}_{M,p-1}, \mathbf{h}_p^\theta, \mathbf{0}_{M,K-p-1}] \tag{56c}$$

$$\partial\bar{\mathbf{B}}/\partial\alpha_p = [\mathbf{0}_{M,p-1}, \mathbf{h}_p^\alpha, \mathbf{0}_{M,K-p-1}] \tag{56d}$$
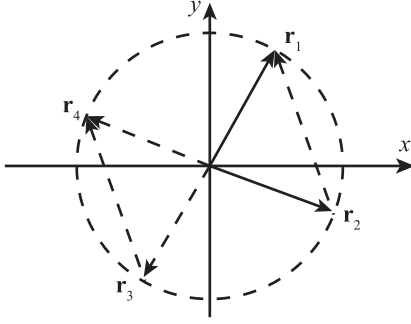
Fig. 10. Geometrical explanation of (55).

with

$$\mathbf{h}_p^{\rho} = [\exp(j\phi_p)\mathbf{a}_p^{rH}\mathbf{D}(\boldsymbol{\beta})]^H \tag{57a}$$

$$\mathbf{h}_p^{\phi} = [jg_p\mathbf{a}_p^{rH}\mathbf{D}(\boldsymbol{\beta})]^H, \tag{57b}$$

$$\mathbf{h}_p^{\theta} = \left[\beta_p \frac{\partial \mathbf{a}^T(\theta_p)}{\partial \theta_p}\mathbf{D}(\mathbf{g}), \beta_p^* \frac{\partial \mathbf{a}^T(\theta_p)}{\partial \theta_p}\mathbf{D}^*(\boldsymbol{\Gamma}\mathbf{g}) \right]^T, \tag{57c}$$

$$\mathbf{h}_p^{\alpha} = \left[j\frac{1}{2}\beta_p\mathbf{a}^T(\theta_p)\mathbf{D}(\mathbf{g}), -j\frac{1}{2}\beta_p^*\mathbf{a}^T(\theta_p)\mathbf{D}^*(\boldsymbol{\Gamma}\mathbf{g}) \right]^T, \tag{57d}$$

where $\mathbf{a}_p^{rH}$ is the pth row of $\mathbf{A}$ and $\mathbf{0}_{m,n}$ denotes $m \times n$ matrix of 0s.

For a concise expression of $\mathbf{F}_0''(\boldsymbol{\mu})$, define the matrix $\mathbf{F} \in \mathbb{C}^{(2M+2K)\times(2M+2K)}$ as

$$[\mathbf{F}]_{pq} = \text{Tr}\left(\mathbf{U}\frac{\partial \bar{\mathbf{B}}^H}{\partial \eta_q}\mathbf{P}_{\bar{\mathbf{B}}}^{\perp}\frac{\partial \bar{\mathbf{B}}}{\partial \eta_p} \right), \tag{58}$$

where η_p is the pth element of $\boldsymbol{\eta}$ $(= [\boldsymbol{\rho}^T, \boldsymbol{\phi}^T, \boldsymbol{\theta}^T, \boldsymbol{\alpha}^T]^T)$. In order to obtain $\mathbf{F}$, we need to derive all the blocks related to these four parameters.

For the gain errors block of $\mathbf{F}$, denoted by $\mathbf{F}_{\rho\rho}$, we have that $1 \leq p, q \leq M$. And its (p, q)th element is given by

$$\begin{aligned} [\mathbf{F}_{\rho\rho}]_{pq} &= \text{Tr}\left(\mathbf{U}(\mathbf{h}_q^{\rho}[\boldsymbol{\Xi}_1]_{qp}\mathbf{h}_p^{\rho H} + \mathbf{h}_q^{\rho*}[\boldsymbol{\Gamma}\boldsymbol{\Xi}_2]_{qp}\mathbf{h}_p^{\rho H} \right. \\ &\quad \left. + \mathbf{h}_q^{\rho}[\boldsymbol{\Xi}_2^H\boldsymbol{\Gamma}]_{qp}\mathbf{h}_p^{\rho T} + \mathbf{h}_q^{\rho*}[\boldsymbol{\Xi}_1^*]_{qp}\mathbf{h}_p^{\rho T}) \right), \\ &= 2[\boldsymbol{\Xi}_1]_{qp}\mathbf{h}_p^{\rho H}\mathbf{U}\mathbf{h}_q^{\rho} + 2[\boldsymbol{\Gamma}\boldsymbol{\Xi}_2]_{qp}\mathbf{h}_p^{\rho H}\mathbf{U}\mathbf{h}_q^{\rho*}, \end{aligned} \tag{59}$$

where $\boldsymbol{\Xi}_1$, $\boldsymbol{\Xi}_2$ are defined in (36), and the second equation uses the facts that $\boldsymbol{\Gamma}\boldsymbol{\Xi}_2 = (\boldsymbol{\Xi}_2^H\boldsymbol{\Gamma})^*$ and $\mathbf{U} \in \mathbb{R}^{K\times K}$ (see the discussion after (34)). It follows that

$$\mathbf{F}_{\rho\rho} = 2(\mathbf{H}_{\boldsymbol{\rho}}^H\mathbf{U}\mathbf{H}_{\boldsymbol{\rho}}) \odot \boldsymbol{\Xi}_1^T + 2(\mathbf{H}_{\boldsymbol{\rho}}^H\mathbf{U}\mathbf{H}_{\boldsymbol{\rho}}^*) \odot (\boldsymbol{\Gamma}\boldsymbol{\Xi}_2)^T \tag{60}$$

where $\mathbf{H}_{\boldsymbol{\rho}} = [\mathbf{h}_1^{\rho}, \mathbf{h}_2^{\rho}, \ldots, \mathbf{h}_M^{\rho}] = (\mathbf{D}(\exp(j\boldsymbol{\phi}))\mathbf{A}\mathbf{D}(\boldsymbol{\beta}))^H$. Similarly, we can get the phase errors block

$$\mathbf{F}_{\phi\phi} = 2(\mathbf{H}_{\boldsymbol{\phi}}^H\mathbf{U}\mathbf{H}_{\boldsymbol{\phi}}) \odot \boldsymbol{\Xi}_1^T + 2(\mathbf{H}_{\boldsymbol{\phi}}^H\mathbf{U}\mathbf{H}_{\boldsymbol{\phi}}^*) \odot (\boldsymbol{\Gamma}\boldsymbol{\Xi}_2)^T \tag{61}$$

and the cross term of the gain errors and phase errors

$$\mathbf{F}_{\rho\phi} = 2(\mathbf{H}_{\boldsymbol{\rho}}^H\mathbf{U}\mathbf{H}_{\boldsymbol{\phi}}) \odot \boldsymbol{\Xi}_1^T + 2(\mathbf{H}_{\boldsymbol{\rho}}^H\mathbf{U}\mathbf{H}_{\boldsymbol{\phi}}^*) \odot (\boldsymbol{\Gamma}\boldsymbol{\Xi}_2)^T, \tag{62}$$

where $\mathbf{H}_{\boldsymbol{\phi}} = [\mathbf{h}_1^{\phi}, \mathbf{h}_2^{\phi}, \ldots, \mathbf{h}_M^{\phi}] = -j\mathbf{B}_1^H$. Construct the gain-phase errors block as $\mathbf{F}_{\mathbf{gg}} = \begin{bmatrix} \mathbf{F}_{\rho\rho} & \mathbf{F}_{\rho\phi} \\ \mathbf{F}_{\rho\phi}^H & \mathbf{F}_{\phi\phi} \end{bmatrix}$. A concise expression of $\mathbf{F}_{\mathbf{gg}}$ shown in (36) immediately follows from (60)-(62).

For the cross term of gain errors and DOAs, denoted by $\mathbf{F}_{\rho\theta}$, we have that $1 \leq p \leq M$ and $1 \leq q - 2M \leq K$. Let $i = q - 2M$. Its (p, i)th element is given by

$$\begin{aligned} [\mathbf{F}_{\rho\theta}]_{pi} &= \text{Tr}\left([\mathbf{U}]_{:i}\mathbf{h}_i^{\theta H}([\boldsymbol{\Xi}_3]_{:p}\mathbf{h}_p^{\rho H} + [\boldsymbol{\Xi}_4\boldsymbol{\Gamma}]_{:p}\mathbf{h}_p^{\rho T}) \right) \\ &= \mathbf{h}_p^{\rho H}[\mathbf{U}]_{:i}[\boldsymbol{\Xi}_3]_{:p}^T\mathbf{h}_i^{\theta*} + \mathbf{h}_p^{\rho T}[\mathbf{U}]_{:i}[\boldsymbol{\Xi}_4\boldsymbol{\Gamma}]_{:p}^T\mathbf{h}_i^{\theta*}, \end{aligned} \tag{63}$$

where $[\cdot]_{:i}$ denotes the ith column, and $\boldsymbol{\Xi}_3$, $\boldsymbol{\Xi}_4$ are defined in (40). It follows that

$$\mathbf{F}_{\rho\theta} = (\mathbf{H}_{\boldsymbol{\rho}}^H\mathbf{U}) \odot (\boldsymbol{\Xi}_3^T\mathbf{H}_{\boldsymbol{\theta}}^*) + (\mathbf{H}_{\boldsymbol{\rho}}^T\mathbf{U}) \odot (\boldsymbol{\Gamma}\boldsymbol{\Xi}_4^T\mathbf{H}_{\boldsymbol{\theta}}^*), \tag{64}$$

where a simplified expression of $\mathbf{H}_{\boldsymbol{\theta}}$ $(= [\mathbf{h}_1^{\theta}, \mathbf{h}_2^{\theta}, \ldots, \mathbf{h}_K^{\theta}])$ is given in (39). Similarly, we can get the cross term related to the gain-phase errors and the parameters of the signals, i.e., $\mathbf{F}_{\mathbf{gs}}$, as shown in (40). Finally, the $\boldsymbol{\theta}$ and $\boldsymbol{\alpha}$ related block, i.e., $\mathbf{F}_{\mathbf{ss}}$, can be easily obtained as shown in (38).

REFERENCES

[1] R. Schmidt, "Multiple emitter location and signal parameter estimation," *IEEE Trans. Antennas Propag.*, vol. 34, no. 3, pp. 276–280, Mar. 1986.

[2] S. Kung, C. Lo, and R. Foka, "A toeplitz approximation approach to coherent source direction finding," in *Proc. IEEE Int. Conf. Acoust. Speech, Signal Process. (ICASSP)*, vol. 11, Apr. 1986, pp. 193–196.

[3] H. Krim and M. Viberg, "Two decades of array signal processing research: The parametric approach," *IEEE Signal Process. Mag.*, vol. 13, no. 4, pp. 67–94, Jul. 1996.

[4] W. Xie, F. Wen, J. Liu, and Q. Wan, "Source association, DOA and fading coefficients estimation for multipath signals," *IEEE Trans. Signal Process.*, vol. 65, no. 11, pp. 2773–2789, Jun. 2017.

[5] F. Wen, Q. Wan, R. Fan, and H. Wei, "Improved MUSIC algorithm for multiple noncoherent subarrays," *IEEE Signal Process. Lett.*, vol. 21, no. 5, pp. 527–530, May 2014.

[6] A. Ferreol, P. Larzabal, and M. Viberg, "Statistical analysis of the MUSIC algorithm in the presence of modeling errors, taking into account the resolution probability," *IEEE Trans. Signal Process.*, vol. 58, no. 8, pp. 4156–4166, Aug. 2010.

[7] D. R. Fuhrmann, "Estimation of sensor gain and phase," *IEEE Trans. Signal Process.*, vol. 42, no. 1, pp. 77–87, Jan. 1994.

[8] Q. Cheng, Y. Hua, and P. Stoica, "Asymptotic performance of optimal gain-and-phase estimators of sensor arrays," *IEEE Trans. Signal Process.*, vol. 48, no. 12, pp. 3587–3590, Dec. 2000.

[9] B. P. Ng, J. P. Lie, M. H. Er, and A. Feng, "A practical simple geometry and gain/phase calibration technique for antenna array processing," *IEEE Trans. Antennas Propag.*, vol. 57, no. 7, pp. 1963–1972, Jul. 2009.

[10] P. S. Naidu, *Sensor Array Signal Processing*, 2nd ed. Boca Raton, FL, USA: CRC Press, 2009.

[11] A. Paulraj, R. Roy, and T. Kailath, "A subspace rotation approach to signal parameter estimation," *Proc. IEEE*, vol. 74, no. 7, pp. 1044–1046, Jul. 1986.

[12] A. J. Weiss and B. Friedlander, "Eigenstructure methods for direction finding with sensor gain and phase uncertainties," *Circuits Syst. Signal Process.*, vol. 9, no. 3, pp. 271–300, Sep. 1990.

[13] A. Swindlehurst, "A maximum *a posteriori* approach to beamforming in the presence of calibration errors," in *Proc. 8th IEEE Signal Process. Workshop Statist. Signal Array Process.*, Corfu Island, Greece, Jun. 1996, pp. 82–85.

[14] M. Viberg and A. L. Swindlehurst, "A Bayesian approach to autocalibration for parametric array signal processing," *IEEE Trans. Signal Process.*, vol. 42, no. 12, pp. 3495–3507, Dec. 1994.

[15] A. Liu, G. Liao, C. Zeng, Z. Yang, and Q. Xu, "An eigenstructure method for estimating DOA and sensor gain-phase errors," *IEEE Trans. Signal Process.*, vol. 59, no. 12, pp. 5944–5956, Dec. 2011.

[16] S. Cao, Z. Ye, D. Xu, and X. Xu, "A Hadamard product based method for DOA estimation and gain-phase error calibration," *IEEE Trans. Aerosp. Electron. Syst.*, vol. 49, no. 2, pp. 1224–1233, Apr. 2013.

[17] M. P. Wylie, S. Roy, and H. Messer, "Joint DOA estimation and phase calibration of linear equispaced LES arrays," *IEEE Trans. Signal Process.*, vol. 42, no. 12, pp. 3449–3459, Dec. 1994.

[18] J. Kim, H. J. Yang, B. W. Jung, and J. Chun, "Blind calibration for a linear array with gain and phase error using independent component analysis," *IEEE Antennas Wireless Propag. Lett.*, vol. 9, no. 1, pp. 1259–1262, 2010.

[19] Y. Li and M. H. Er, "Theoretical analyses of gain and phase error calibration with optimal implementation for linear equispaced array," *IEEE Trans. Signal Process.*, vol. 54, no. 2, pp. 712–723, Feb. 2006.

[20] B. Liao and S. C. Chan, "Direction finding with partly calibrated uniform linear arrays," *IEEE Trans. Antennas Propag.*, vol. 60, no. 2, pp. 922–929, Feb. 2012.

[21] B. Liao and S.-C. Chan, "Direction-of-arrival estimation in subarrays-based linear sparse arrays with gain/phase uncertainties," *IEEE Trans. Aerosp. Electron. Syst.*, vol. 49, no. 4, pp. 2268–2280, Oct. 2013.

[22] B. Liao and S. C. Chan, "Direction finding in partly calibrated uniform linear arrays with unknown gains and phases," *IEEE Trans. Aerosp. Electron. Syst.*, vol. 51, no. 1, pp. 217–227, Jan. 2015.

[23] P. Heidenreich, A. M. Zoubir, and M. Rubsamen, "Joint 2-D DOA estimation and phase calibration for uniform rectangular arrays," *IEEE Trans. Signal Process.*, vol. 60, no. 9, pp. 4683–4693, Sep. 2012.

[24] M. Haardt and J. A. Nossek, "Unitary ESPRIT: How to obtain increased estimation accuracy with a reduced computational burden," *IEEE Trans. Signal Process.*, vol. 43, no. 5, pp. 1232–1242, May 1995.

[25] W. Xie, X. Y. Zhang, L. B. Chen, J. H. Yin, and Q. Wan, "Fast DOA estimation algorithm for noncircular sources with central symmetrical array," in *Proc. 12th Int. Conf. Signal Process. (ICSP)*, Oct. 2014, pp. 267–270.

[26] M. Haardt and F. Romer, "Enhancements of unitary ESPRIT for non-circular sources," in *Proc. IEEE Int. Conf. Acoust. Speech, Signal Process.*, vol. 2. Montreal, QC, Cannada, May 2004, pp. 101–104.

[27] P. J. Schreier and L. L. Scharf, *Statistical Signal Processing of Complex-Valued Data: The Theory of Improper and Noncircular Signals*. Cambridge, U.K.: Cambridge Univ. Press, 2010.

[28] J.-P. Delmas and H. Abeida, "Stochastic Cramér–Rao bound for noncircular signals with application to DOA estimation," *IEEE Trans. Signal Process.*, vol. 52, no. 11, pp. 3192–3199, Nov. 2004.

[29] F. Römer and M. Haardt, "Deterministic Cramér–Rao bounds for strict sense non-circular sources," in *Proc. IEEE Workshop Smart Antennas*, Vienna, Austria, Jan. 2007, pp. 1–5.

[30] H. Abeida and J.-P. Delmas, "MUSIC-like estimation of direction of arrival for noncircular sources," *IEEE Trans. Signal Process.*, vol. 54, no. 7, pp. 2678–2690, Jul. 2006.

[31] D. Astely, A. L. Swindlehurst, and B. Ottersten, "Spatial signature estimation for uniform linear arrays with unknown receiver gains and phases," *IEEE Trans. Signal Process.*, vol. 47, no. 8, pp. 2128–2138, Aug. 1999.

[32] F. Roemer and M. Haardt, "Efficient 1-D and 2-D DOA estimation for non-circular sourceswith hexagonal shaped ESPAR arrays," in *Proc. IEEE Int. Conf. Acoust. Speech, Signal Process. (ICASSP)*, vol. 4, May 2006, pp. 881–884.

[33] B. Ottersten, M. Viberg, and T. Kailath, "Analysis of subspace fitting and ML techniques for parameter estimation from sensor array data," *IEEE Trans. Signal Process.*, vol. 40, no. 3, pp. 590–600, Mar. 1992.

[34] B. Hochwald and A. Nehorai, "Concentrated Cramer–Rao bound expressions," *IEEE Trans. Inf. Theory*, vol. 40, no. 2, pp. 363–371, Mar. 1994.

[35] P. Stoica and A. Nehorai, "Performance study of conditional and unconditional direction-of-arrival estimation," *IEEE Trans. Acoust., Speech Signal Process.*, vol. 38, no. 10, pp. 1783–1795, Oct. 1990.

[36] B. Friedlander and A. J. Weiss, "Performance of direction-finding systems with sensor gain and phase uncertainties," *Circuits Syst. Signal Process.*, vol. 12, no. 1, pp. 3–35, Mar. 1993.
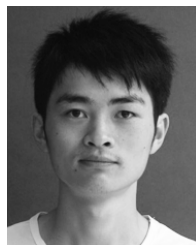
Wei Xie (S'17) was born in Neijiang, China, in 1989. He received the B.S. degree in electronic information science and technology from Yantai University, Yantai, China, in 2011. He is currently pursuing the Ph.D. degree with the School of Electronic Engineering, University of Electronic Science and Technology of China, Chengdu, China. His research interests include array signal processing, sparse signal representation, and radio localization.

Changsheng Wang (S'17) is currently pursuing the Ph.D. degree with the School of Electronic Engineering, University of Electronic Science and Technology of China, Chengdu, China. His research interests include array signal processing and signal recognition.
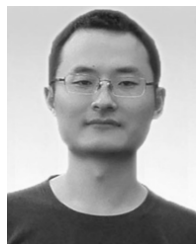
Fei Wen (M'15) received the B.S. degree and the Ph.D. degree in communications and information engineering from the University of Electronic Science and Technology of China, in 2006 and 2013, respectively. Since 2012, he has been a Lecturer with Air Force Engineering University. Now he is a Research Fellow with the Department of Electronic Engineering, Shanghai Jiao Tong University. His main research interests are statistical signal processing and nonconvex optimization.
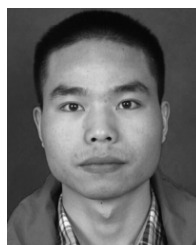
Jiangbo Liu (S'17) received the B.S. degree in information and computing science from Yanbian University, Jilin, China, in 2012. He is currently pursuing the Ph.D. degree with the University of Electronic Science and Technology of China. His research interests are in array signal processing especially the robust adaptive beamforming.

Qun Wan (M'04) received the B.Sc. degree in electronic engineering from Nanjing University in 1993, and the M.Sc. and Ph.D. degrees in electronic engineering from the University of Electronic Science and Technology of China (UESTC), in 1996 and 2001, respectively. From 2001 to 2003, he held a post-doctoral position with the Department of Electronic Engineering, Tsinghua University. Since 2004, he has been a Professor with the Department of Electronic Engineering, UESTC. He is currently the Director of the Joint Research Lab of Array Signal Processing and an Associate Dean of the School of Electronic Engineering. His research interests include direction finding, radio localization, and signal processing based on information criterion.